heritage

MDPI

*Article*

# The Role of Metallography in the Study of Archaeological Metal Votive Statuettes from the National Archaeological Museum of Campobasso

**Camilla Criaco [1], Davide Delfino [2], Roberto Spotorno [1] and Paolo Piccardo [1,3,*]**

[1] Dipartimento di Chimica e Chimica Industriale, Università di Genova, 16146 Genova, Italy; camilla.criaco@edu.unige.it (C.C.); roberto.spotorno@unige.it (R.S.)
[2] Museo Archeologico Nazionale di Campobasso, Parco Archeologico di Sepino-Direzione Regionale Musei Molise, 86100 Campobasso, Italy; davide.delfino@cultura.gov.it
[3] Archéosciences Bordeaux, UMR 6034, Université Bordeaux Montaigne, CNRS, F-33607 Pessac Cedex, France
* Correspondence: paolo.piccardo@unige.it

**Abstract**

This study presents the first metallurgical analysis of twenty-five votive statuettes of Hercules from the National Archaeological Museum of *Campobasso*, *Molise*, Italy. These artifacts, which have previously been unexamined from a metallurgical perspective, were analyzed to understand their composition, manufacturing techniques, and current state of preservation. All the samples were first analyzed in situ using X-ray fluorescence (XRF) and then were sampled to conduct microstructural analyses on polished cross-sections by optical and scanning electron microscopy. The statuettes revealed a ternary Cu-Sn-Pb alloy, consistent with historical alloying practices and manufacturing techniques typical of the period. The study highlights a homogeneous biphasic microstructure with dispersed lead nodules within the bronze matrix. The corrosion products on the surface have peculiar colors and textures due to both the finishing process and the alteration accord over centuries of abandonment, aiding the understanding of the material's behavior over time. The compositional results confirm the usage of materials and techniques in line with other coeval artifacts.

**Keywords:** bronze; metallography; compositional analyses; reproduction; corrosion; votive statuettes; Italic archeology

## 1. Introduction

Archaeological museums often present visitors with a wide range of metal artifacts from various eras, geographical locations (archaeological sites, neighboring regions, etc.), chronological information, and historical details about the objects displayed in show cases. However, it is rare for museums to address the material aspects of the objects themselves, such as the explicit composition of metal materials other than general terms like bronze, the techniques used in their production, or specific characteristics of the metal alloys, insights that a scientific, chemical, and metallographic approach can reveal. These aspects not only enhance the understanding of cultural heritage for visitors, who can appreciate how metals serve as solid-state memories of the past, but also benefit specialists in the field, such as conservators, curators, and restorers, who can use optimized protocols for the conservation and restoration of these valuable artifacts. This paper presents the study of twenty-five votive statuettes of Hercules (Figure 1), a demigod venerated by the Samnites, an ancient

Check for updates

Academic Editor: Antonio Brunetti

Received: 3 November 2025
Revised: 1 December 2025
Accepted: 8 January 2026
Published: 9 January 2026

**Copyright:** © 2026 by the authors. Licensee MDPI, Basel, Switzerland. This article is an open access article distributed under the terms and conditions of the Creative Commons Attribution (CC BY) license.

Italic civilization living in *Samnium* and long-standing rivals of the Romans (IV century BC-I century AD). These artifacts, coming from known and unknown archaeological sites of *Molise* region and preserved at the National Archaeological Museum of *Campobasso* [1] are analyzed from a chemical, metallurgical, and material perspective, representing the first study of metallic artifacts conserved in *Molise*, Italy. This study aims to contribute to the quest to rebuild the manufacturing processes behind the creation of the finished objects by analyzing compositional data on the alloys and their microstructures. This approach provides insight into the selection of materials and techniques used, allowing the formulation of hypotheses based on the manufacturing process through observation of the microstructures. At the same time, the investigation protocol is supported by further experimental activities driven by the preliminary characterization of the archaeological specimen. Furthermore, at least preliminarily, this study offers the opportunity to investigate the corrosion products formed on the artifacts during the abandonment period. This helps to understand the behavior of certain alloy elements and their reactions with both the depositional and external environments, thus enabling the development of a conservation and potential restoration protocol useful for experts in the field. Furthermore, it aims to understand the artisans' choices regarding the aesthetic appearance of the finished objects, whether intentional or not, based on the distinctive colors observed on the surface of the statuettes. This research is the first step in filling a critical gap in the metallurgical study of *Molise*'s archaeological heritage, offering a foundation for further exploration into ancient craftsmanship within the region.




**Figure 1.** Some of the votive statuettes housed at the National Archaeological Museum of *Campobasso* (*Italy*).

## 2. Materials and Methods

### *2.1. Historical Context and Description of the Statuettes*

The twenty-five statuettes are dated between the 5th and 1st centuries BCE and generally lack precise geographical origins, with only a few associated with specific archaeological sites of the *Molise* region. The earliest attempt to document these materials was made by *Antonio Sogliano* [2], who in 1889 compiled the first inventory of the *Museo Provinciale Sannitico* (*Campobasso*, *Molise*, *Italy*). Although fundamental as a historical record,

his catalogue reflects the antiquarian practices of the time and provides limited contextual and typological detail.

A more rigorous and archaeology-oriented reassessment was carried out by Angela Di Niro [3], whose 2007 catalogue offers updated classifications, improved documentation, and more reliable provenance attributions. Building on this foundation, recent studies by Davide Delfino and Viviana Carbonara [4] have further refined the interpretation of specific artefact classes and introduced modern museological approaches, integrating the collection into broader research on Italic material culture. Together, these successive contributions have progressively transformed the museum's holdings from a loosely documented assemblage into a coherent and analytically valuable corpus.

These statuettes depict Hercules, the demigod symbolizing strength and perseverance, a revered figure among Italic populations influenced by neighboring Greek culture. Some of the statuettes were originally part of private collections, donated to *Campobasso* in the late 19th century when the first National Archaeological Museum of *Campobasso* was founded. This makes it quite difficult, if not impossible, to locate the finding coordinates, which would make it possible to create a connection among pieces, eventually. As a matter of fact, few of these pieces have documented archaeological contexts, such as *Trivento*; others likely originated from clandestine excavations before being acquired by private collectors. The artifacts were cataloged, partially restored, and publicly displayed. Until now, studies have focused on these statuettes' historical and archaeological context; this research is the first to investigate their chemical and material properties. Typically associated with sacred spaces, such as temples, the statuettes feature Hercules in two standard poses: resting and attacking. In the resting pose, Hercules stands upright with arms relaxed, sometimes wearing the lion skin (*leontè*), symbolic of his heroism, representing periods of peace. On the other hand, the attacking pose shows Hercules in a dynamic position, wielding a club with one arm raised and either holding or wearing the *leontè* as a distinctive mark, a stance associated with wartime [5]. Most of the statuettes are characterized by a relatively simple design, although some have finer craftsmanship, with the Hercules of *Trivento* (Herc_1002 Figure 1) as the best example. Each piece measures between 9 cm and 15 cm in height, and they display thick and homogenous corrosion patinas with a range of colors, exhibiting a broad chromatic variability. Most pieces display green patinas, ranging from pale to dark shades. Gray surfaces, both light and dark, also occur within the corpus, though less frequently, while whitish tones are comparatively rare. A distinct subset is characterized instead by a pronounced brown coloration. The distribution of these hues (7 green, 9 gray, 2 whitish, and 7 brown examples) highlights the considerable heterogeneity of the surface patinas.

### *2.2. Conservation Degree and Metallurgical State*

The specimens were at first carefully analyzed macroscopically to assess their conservation state and to facilitate subsequent data collection and microscopic analysis. This phase is essential, as it enables observation of the alloy's composition, even thoroughly semiquantitative due to the thick layer of patina. The possibility offered by some of the statuettes to sample a little fragment opens the opportunity to further investigate the chemical nature of the patina and the metal substrate. The alloy is also characterized by its metallographic features, such as microstructure, phases, inclusions, and any thermal and/or mechanical treatments. Together, these data allow for the reconstruction of the likely processes applied to the material.

### *2.3. From Specimen Collection to Microscopic Analyses*

The group of twenty-five votive statuettes of Hercules was first analyzed in situ, starting with a macroscopic examination to assess their integrity, conservation state, and

the quality and color of the corrosion patinas covering them. Preliminary compositional analysis was then conducted using a DELTA Professional Olympus portable XRF (Waltham, MA, USA, X-ray fluorescence 2 beams nkV xtime, n'kv ytime). This type of analysis provided an initial data set on-site, allowing us to avoid relocating the objects to another facility, thus reducing risks (e.g., accidental damage, theft, or loss). Ideally, XRF analysis requires surface cleaning or pre-polishing to remove corrosion patinas that could affect the data. Fortunately, exposed alloy areas without corrosion patina were available, enabling analysis at multiple points on each statuette, without any surface preparation before the analysis procedure. As a second step, micro-sampling was conducted on a carefully chosen selection of statuettes to prevent structural or aesthetic damage to the artifacts. The sampling described in Table 1 was carried out in areas that were already visibly damaged or not intact on the back of the object and therefore not visible, such as behind the knee, the ankles, the wrists, or the forearms. Samples, approximately 2–5 mm in size, were carefully trimmed using a precision saw and then mounted in cold-curing epoxy resin. Afterward, the samples were cleaned and polished to prepare them for subsequent microscopic examination. These procedures were carried out using Struers' TegraForce-5 equipment (Struers, Ballerup, Denmark), with a sequence of grinding papers (silicon carbide, SiC) of progressively finer grit sizes, ranging from 180 to 1000 grit, and using water as both coolant and lubricant. Then, fabric discs were used with a diamond suspension of granulometry ranging from 6 µm to ¼ µm, step by step. The finishing step was made by hand using ¼ µm polycrystalline diamond spray until the removal of artifacts and defects.

**Table 1.** Samples and analyses performed. "X" indicates that the analysis was carried out.

| N. Hercules | p-XRF | Sampling | LOM | SEM |
|---|---|---|---|---|
| Herc_1 | X | X | X | X |
| Herc_2 | X | | | |
| Herc_3 | X | | | |
| Herc_4 | X | X | X | X |
| Herc_5 | X | | | |
| Herc_6 | X | X | X | X |
| Herc_1002 | X | | | |
| Herc_1005 | X | X | X | X |
| Herc_1006 | X | X | X | X |
| Herc_1009 | X | X | X | X |
| Herc_1013 | X | X | X | X |
| Herc_1014 | X | | | |
| Herc_1019 | X | | | |
| Herc_1025 | X | X | X | X |
| Herc_1028 | X | X | X | X |
| Herc_1031 | X | | | |
| Herc_1033 | X | | | |
| Herc_1035 | X | | | |
| Herc_4137 | X | X | X | X |
| Herc_6748 | X | X | X | X |
| Herc_34904 | X | | | |
| Herc_34905 | X | | | |
| Herc_34906 | X | | | |
| Herc_42491 | X | | | |
| Herc_58342 | X | X | X | X |

The investigation was conducted using the following microscopical techniques:

1. Optical microscopy in both bright and dark fields (using Leica MEF4 M equipped with six magnifications: 25×, 50×, 100×, 200×, 500×, 1000×, Wetzlar; Germany).

2. Energy Dispersive X-ray spectroscopy (using a PENTAFET® EDXS detector (Oxford Instruments, Abingdon, UK) sensitive to light elements), connected to a Scanning Electron Microscope (SEM) Evo40 Zeiss (Oxford Instruments, Abingdon-on-Thames, UK) and INCA 300 software (version 7.3) for BSE (backscattered electrons).

Polished surfaces observed at the Light Optical Microscope (LOM) in Bright Field showed nodules of lead, and corrosion, but no signs of cracking or intergranular corrosion. The Dark Field (contrast method on LOM), on the other hand, by its contrast, highlights different colors of the corrosion products depending on their nature and composition. In this study, etching was performed using an alcoholic ferric chloride solution, composed of 3 g of $FeCl_3$, 1 mL of HCl, and 97 mL of anhydrous ethyl alcohol. To optimize the etching process, the solution was further diluted 1:1 with additional anhydrous ethyl alcohol.

The samples were made conductive through Au coating for the observations and compositional analyses were performed with SEM-EDS. These analyses allow for the determination of the elemental composition of the studied alloy and high-magnification microscopic observations of its microstructure. In doing so, an overall biphasic homogeneous alloy was generally observed, rich in dispersed Pb nodules. Table 1 lists the samples and the types of analyses they underwent, and Figures 2 and 3 show the selected areas of material sampling.

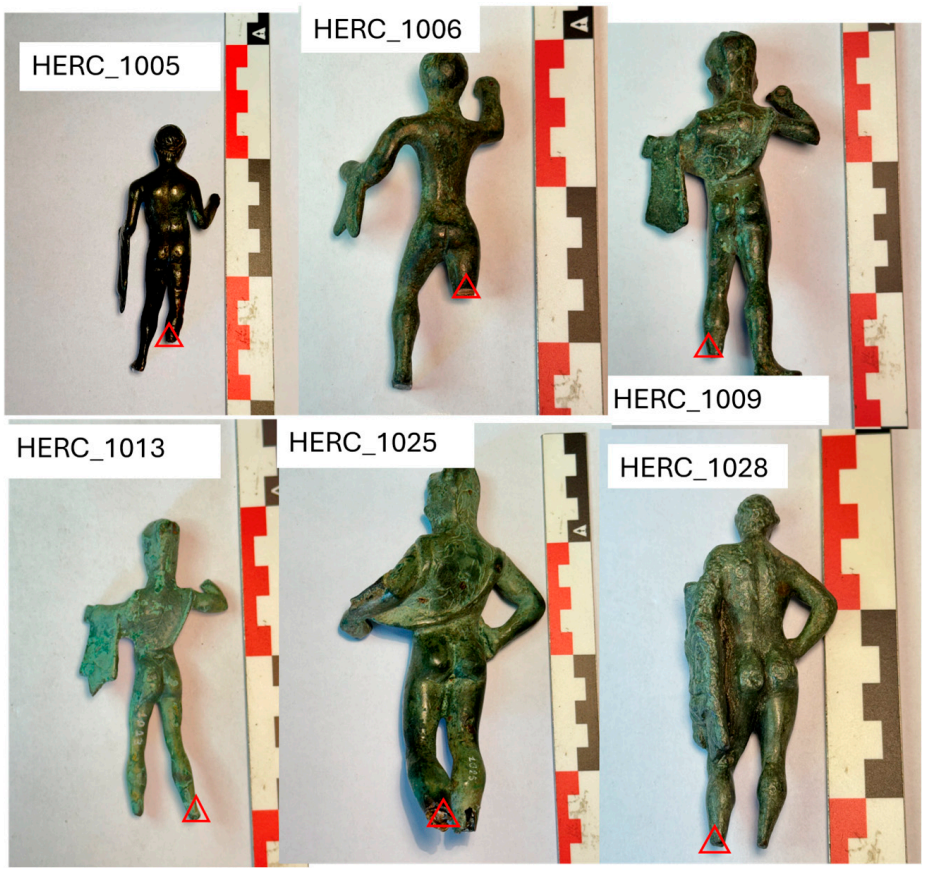



**Figure 2.** First sampling set with a detailed indication (red triangle) of the area from which the sample was taken.




**Figure 3.** Second sampling set with a detailed indication (red triangle) of the area from which the sample was taken.

## 3. Results and Discussion

To ensure maximum clarity and readability, the results are divided into two different sections: Compositional Analyses and Metallography.

### *3.1. p-XRF Results*

Analyses began with in situ p-XRF. Although XRF analysis typically measures surface composition (~10 microns in depth for alloy samples), and surfaces that are painted, plated, corroded, or peened may require additional preparation or grinding, in these cases, it was feasible to analyze areas of the artifacts where he patina is thin enough to make visible the underlying alloy. Further, without subjecting the statuettes to any cleaning or preparatory process, this made possible to analyze various exposed alloy areas to obtain the maximum results.

Direct observation approach preserved the objects while enabling the extraction of preliminary data for composition (Table 2).

The very high Sn and Pb content is related to the impact of the surface patina (even though thin enough to show the substrate) when such elements are naturally in higher relative concentrations than in the alloy. The long-lasting corrosion process in specific environments, such as the soil, leads to the initial formation of Cu rich oxidized products that react with the surrounding medium, causing the diffusion of Cu ions while Pb and

Sn tend to remain in the patina. The consequence of this process is that the patina is commonly Sn and Pb richer than the alloy [6]. However, the surface finishing, the intrinsic composition of the alloy (as revealed by the SEM-EDX) applied to the polished cross-section, and possible casting practices might have further enhanced this phenomenon, as discussed in the following chapter.

**Table 2.** p-XRF results.

| N. Hercules | Cu * | Sn * | Pb * |
|---|---|---|---|
| Herc_1 | 35 ± 0.1 | 49 ± 0.2 | 17 ± 0.1 |
| Herc_2 | 50 ± 0.1 | 13 ± 0.1 | 37 ± 0.1 |
| Herc_3 | 62 ± 0.1 | 19 ± 0.1 | 19 ± 0.1 |
| Herc_4 | 47 ± 0.1 | 29 ± 0.1 | 24 ± 0.1 |
| Herc_5 | 52 ± 0.1 | 24 ± 0.1 | 23 ± 0.1 |
| Herc_6 | 34 ± 0.1 | 18 ± 0.1 | 48 ± 0.1 |
| Herc_1002 | 50 ± 0.1 | 15 ± 0.1 | 35 ± 0.1 |
| Herc_1005 | 51 ± 0.1 | 20 ± 0.1 | 29 ± 0.1 |
| Herc_1006 | 81 ± 0.1 | 7 ± 0.1 | 12 ± 0.1 |
| Herc_1009 | 52 ± 0.1 | 19 ± 0.1 | 29 ± 0.1 |
| Herc_1013 | 36 ± 0.1 | 44 ± 0.1 | 20 ± 0.1 |
| Herc_1014 | 45 ± 0.1 | 22 ± 0.2 | 34 ± 0.1 |
| Herc_1019 | 69 ± 0.1 | 15 ± 0.1 | 16 ± 0.1 |
| Herc_1025 | 40 ± 0.1 | 27 ± 0.1 | 33 ± 0.1 |
| Herc_1028 | 36 ± 0.1 | 16 ± 0.1 | 48 ± 0.1 |
| Herc_1031 | 39 ± 0.1 | 18 ± 0.1 | 43 ± 0.1 |
| Herc_1033 | 39 ± 0.1 | 21 ± 0.2 | 40 ± 0.1 |
| Herc_1035 | 54 ± 0.1 | 41 ± 0.1 | 5 ± 0.1 |
| Herc_4137 | 47 ± 0.1 | 16 ± 0.2 | 37 ± 0.2 |
| Herc_6748 | 45 ± 0.1 | 17 ± 0.1 | 38 ± 0.1 |
| Herc_34904 | 31 ± 0.1 | 60 ± 0.1 | 9 ± 0.1 |
| Herc_34905 | 54 ± 0.1 | 38 ± 0.1 | 8 ± 0.1 |
| Herc_34906 | 31 ± 0.1 | 30 ± 0.1 | 39 ± 0.1 |
| Herc_42491 | 46 ± 0.1 | 22 ± 0.1 | 32 ± 0.1 |
| Herc_58342 | 31 ± 0.1 | 56 ± 0.1 | 13 ± 0.1 |

* weight normalized (wt%) and errors as indicated by the instrument.

### *3.2. SEM-EDS Results*

Ancient copper-based alloys generally contain varying amounts of Sn, ranging from a minimum of 1 wt% up to 16 wt%. When Sn content is higher up to exceeding this limit, up to 23 wt% forms new phases [7]. Adding a third or fourth element to the alloy, such as Pb, could be considered unintentional if the concentration is around 1–2 wt%, as it is relatively low (and could be attributed to impurities from the mineral extraction processes). However, when higher percentages are found, it can be regarded as a deliberately added element with specific purposes, as previously mentioned. Compositional analyses conducted using SEM provided detailed data on the elemental composition of the samples. The results can be found in Table 3. Figure 4 also reports on the Cu/Sn ratio with the corresponding distribution.

From the data shown in Figure 5, the Sn concentrations ranging between 5 wt% and 16 wt% fall within the standards observed for the historical period. Similarly, the Pb concentrations, also ranging between 5 wt% and 16 wt%, align with the correct standards [7]. This is partly due to the intrinsic properties of lead, which make it an element intentionally added to the alloy during the creative process of statue-making.

**Table 3.** SEM-EDS results of the metallic samples taken from the statuettes.

| N. Sample | Cu * | Sn * | Pb * | Cu **/Sn ** |
|---|---|---|---|---|
| Herc_1 | 78 ± 0.3 | 8 ± 0.3 | 14 ± 0.4 | 91/9 |
| Herc_4 | 75 ± 0.3 | 10 ± 0.3 | 15 ± 0.4 | 88/12 |
| Herc_6 | 82 ± 0.4 | 9 ± 0.3 | 10 ± 0.3 | 90/10 |
| Herc_1005 | 79 ± 0.3 | 5 ± 0.4 | 16 ± 0.5 | 94/6 |
| Herc_1006 | 83 ± 0.4 | 8 ± 0.3 | 9 ± 0.3 | 91/9 |
| Herc_1009 | 86 ± 0.4 | 8 ± 0.3 | 6 ± 0.3 | 91/9 |
| Herc_1013 | 82 ± 0.4 | 9 ± 0.3 | 8 ± 0.3 | 90/10 |
| Herc_1025 | 79 ± 0.3 | 6 ± 0.4 | 15 ± 0.4 | 93/7 |
| Herc_1028 | 79 ± 0.3 | 8 ± 0.3 | 12 ± 0.4 | 91/9 |
| Herc_4137 | 84 ± 0.4 | 9 ± 0.3 | 7 ± 0.3 | 90/10 |
| Herc_6748 | 78 ± 0.3 | 7 ± 0.3 | 15 ± 0.4 | 92/8 |
| Herc_58342 | 79 ± 0.3 | 16 ± 0.5 | 5 ± 0.3 | 83/17 |

* weight normalized (wt%) and errors reported. ** lead-excluded normalized weight.

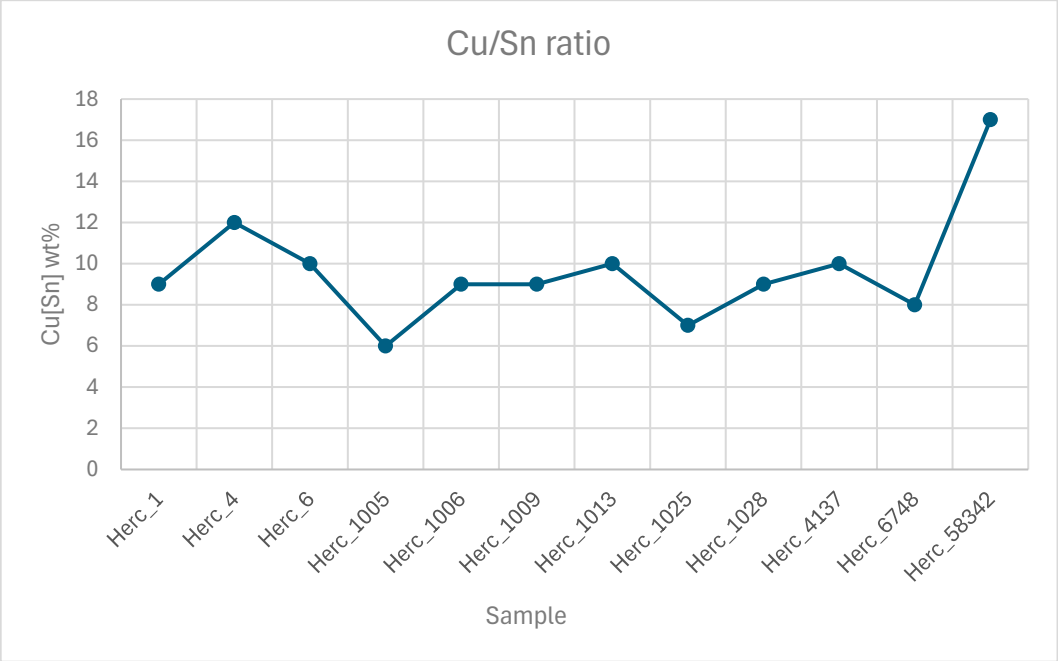



**Figure 4.** Cu/Sn ratio distribution of the analyzed samples. The ratio between 5 wt% and 16 wt% is in line with the historical standard of the period under examination.

As previously discussed, in CuSnPb alloys, only Sn dissolves into Cu lattice as a substitutional alloying element while Pb remains isolated in the form of nodules filling the intergranular cavities. All properties directly related to the alloy are thus affected by Sn content, while Pb plays a marginal role, mainly connected to the solution of continuity in the metal matrix due to its presence. Moreover Cu/Sn ratio represents the alloy targeted and Pb is the element added to further lower the melting point while increasing the weight and, as mentioned, the castability. The percentage of tin reflects technological choices that were often consistent with specific historical periods. A Cu/Sn ratio close to 90:10 is frequently encountered, as it provides a balance between mechanical strength and ease of processing. When the tin content increases beyond this ratio, the alloy tends to become harder but also more difficult to be cold worked and less cost-effective being tin rarer than Cu and Pb. It is crucial to note that Cu/Sn ratio directly affects the formation of metallurgical phases such a $\alpha$-Cu, a Sn-in-Cu solid solution, and, at higher Sn concentrations, intermetallic phases such as $\delta$ and $\varepsilon$, which are associated with a decrease in ductility and increased hardness [7–9].

Table 4 presents the compositional analyses performed on the corrosion patinas of the samples. Understanding the composition of the corrosion products can indeed be crucial for the conservation and restoration of the objects themselves. The increase in the relative content of Sn and Pb observed by the p-XRF is confirmed.

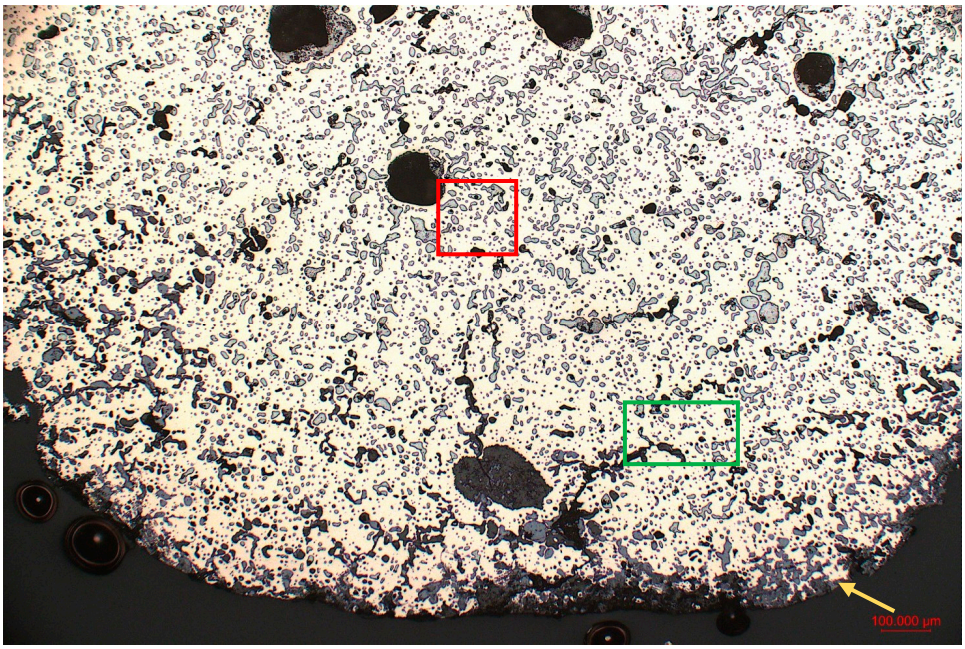



**Figure 5.** LOM image: Brightfield, Herc_ 6, 100×, Homogeneous biphasic structure, Pb nodules (red-marked box), porosities (green-marked box), oxidized products (golden-marked arrow).

**Table 4.** SEM-EDS results of corrosion products.

| N. Sample | O * | Si * | Cl * | Fe * | Cu * | Sn * | Pb * | Ca * |
|---|---|---|---|---|---|---|---|---|
| Herc_1 | XXXX | X | X | X | XXXX | XXXX | X | XXXX |
| Herc_4 | XXX | X | X | | XXXXX | XXX | XXX | |
| Herc_6 | XXXX | X | X | | XXXX | X | XXXX | |
| Herc_1005 | XX | X | X | | XXX | XX | XXXX | X |
| Herc_1006 | X | X | X | X | XXXX | X | XXX | |
| Herc_1009 | X | X | X | X | XXX | XX | XXXX | |
| Herc_1013 | XX | X | X | | XXXX | XX | XX | |
| Herc_1025 | XX | | | X | XXXXX | X | XX | |
| Herc_1028 | X | X | X | | XXXXXX | X | X | X |
| Herc_4137 | XX | X | X | | XXXXX | XX | X | |
| Herc_6748 | XX | X | X | X | XX | XXX | XXX | |
| Herc_58342 | XXX | X | X | X | XX | XXX | X | |

* "X" indicates the presence of corrosion products; an increasing number of "X"s corresponds to higher amounts.

As evidenced in Tables 2 and 3, the compositional data obtained by portable XRF and SEM–EDS display systematic discrepancies across nearly all analysed specimens. Sample Herc_1005 is representative of this broader trend: pXRF reports Cu ≈ 51 wt%, Sn ≈ 20 wt%, and Pb ≈ 29 wt%, whereas SEM–EDS yields Cu ≈ 79 wt%, Sn ≈ 5 wt%, and Pb ≈ 16 wt%. Discrepancies of this magnitude cannot be ascribed to analytical variability alone and instead reflect the fundamentally different interaction volumes and methodological sensitivities of the two techniques in the presence of corrosion-derived surface heterogeneity.

This pattern is fully consistent with the corrosion stratigraphy characteristic of Cu–Sn–Pb alloys in burial environments. Owing to its higher electrochemical reactivity, Cu undergoes

preferential oxidation, generating corrosion phases (e.g., cuprite, hydroxychlorides, carbonates) that can exhibit varying degrees of solubility and mobility [10]. Their progressive transformation and interaction with the burial matrix facilitate the outward diffusion and depletion of Cu from the outermost layers. In contrast, Sn and Pb form highly stable and minimally mobile oxides ($SnO_2$, PbO), which accumulate within the corrosion patina as the corrosion front advances. This leads to a fractionated, compositionally altered surface layer enriched in Sn and Pb and depleted in Cu, a condition observed recurrently in the analysed assemblage. Because portable XRF interrogates a substantially larger and more heterogeneous sampling volume, often extending tens to hundreds of micrometers depending on excitation conditions, it inevitably integrates the signal from this enriched patina with that of the underlying metal [11]. The resulting spectra therefore exhibit systematic overestimation of Sn and Pb and underestimation of Cu, as seen not only in Herc_1005 but in the majority of samples. SEM–EDS, by contrast, operates with a much smaller electron interaction volume (typically 1–2 μm) and, when conducted on polished cross-sections or metallographically prepared surfaces, can selectively target unaltered metallic regions. Consequently, SEM–EDS yields values that more reliably approximate the primary alloy composition and align with expected metallurgical ranges for the corresponding chronological context. Thus, the recurrent divergence between pXRF and SEM–EDS across the dataset reflects not instrumental inconsistency but the distinct penetration depths, matrix effects, and sensitivity to corrosion stratigraphy inherent to each analytical method [12].

### *3.3. Metallography*

Metallographic analysis could be essential for the investigation and research of ancient metallic artifacts: Looking at the microstructures, it is possible to investigate different fields of interest that are strictly connected to the metallurgical features of the materials. For example, it allows us to observe: the grain size and the shape, the different phases and their distribution related to the cooling rate during the solidification process which depends on the mold materials (e.g., its thermal conductivity) among other things, but also mechanical deformation (e.g., shaping to remove defects of casting, stress during solidification, and polishing, etc.) and eventual thermal treatment (e.g., annealing). All these features could change the microstructure without affecting the composition of the alloy, opening different scenarios for the formulation of hypotheses upon which we can tell the history of the final object under investigation. It could also be useful to study the corrosion products on the surface of the findings because they offer the possibility of understanding the reactivity of the metal itself and its behavior depending on the conservation status and the conservation parameters [13].

Figure 5 was taken from Herc_6 and is representative of most of the studied cross-sections. It represents a homogeneous biphasic structure with an α bronze matrix where Pb nodules (within the red-marked box) are dispersed in the intergranular areas. The porosities are visible in black (within the green-marked box), while the dark gray phase nearby the edge of the sample is oxidized products (within the golden-marked arrow).

Details at higher magnification are visible in SEM micrographs: the homogenous, predominantly biphasic structure is confirmed and Pb nodules are noticeably visible in the metallic matrix of all the samples as white zones (within the red-marked box), thanks to the BSE contrast method (Figure 6). Since Pb is insoluble in Cu, it forms these structures, which often exhibit different classes of morphology and size. This could indicate different phases caused by the cooling rate of the alloy, as well as the presence of Pb, which has a relatively low melting point. It is important to focus on the Pb because it forms a liquid phase that remains molten up to the solidification temperature of lead, creating a peritectic, as shown in the Cu-Sn-Pb diagram phases (Figure 7). This indicates that lead creates a

dispersion within the solid copper or bronze matrix. Based on what has been discussed, we can observe these images where a particular phenomenon is noticeable in Figure 8, (within the golden-marked area) when the Pb captured in porosity interconnected with the surface can force molten Pb to spread to the surface while the remaining lead is trapped in the body of the alloy and counteracting mechanically to the thermal contraction of the alloy. The CuSnPb microstructure, indeed, mimics the aspect of a sponge when the CuSn matrix is the sponge itself and the molten Pb is the fluid absorbed in the sponge cavities. This microstructure is formed at high T (≈1000 °C according to the phase diagram) and remains till the solidification of Pb-rich phase at 300 °C. During the cooling of Cu/Sn matrix, the whole volume shrinks according to the thermal expansion/contraction law of the alloy. Thus, when the cavities of the sponge are connected to the surface, the molten Pb-rich phase rises in the free area of the surface between the object and mold wall. All the cavities filled with this fluid of molten Pb-rich phase instead suffer the compression of the shrinking, and the molten Pb responds with equal and opposite force according to the physics of fluids [14,15]. These compressive forces, counterbalanced by equal and opposite forces, induce mechanical stress in the matrix, resulting in mechanical twins as sleeping bonds, lead skin forms, giving it a grey color due to depletion [16]. The phenomenon was further investigated and more clearly revealed through the application of metallographic etching. This chemical treatment enhances the visibility of microstructural features in metallic matrices otherwise obscured by a thin layer of amorphous metal, typically formed during the final stages of mechanical polishing. The choice of etchant depends on the specific composition of the alloy to be examined. Generally, a diluted solution with low aggressiveness is preferred, as it selectively removes the amorphous surface layer without significantly altering the underlying structure. This enables the etchant to first attack the grain boundaries and subsequently reveal individual grains according to their orientation to the observation surface. Metallographic etching is highly sensitive to the chemical reactivity of different phases, preferentially highlighting more reactive zones. As a result, it can reveal residual heterogeneities in the solid solution and provide valuable information about crystallographic orientations. The features observed in Figures 9 and 10 correspond to the phenomena previously described. A marked segregation of lead toward the outer regions of the sample is visible (within the golden-marked arrows), illustrating a compositional gradient from the core, enriched in copper and tin, to the periphery, which is rich in lead [17]. This is indicative of interdendritic segregation, a well-documented process in multiphase systems where low-melting-point constituents such as Pb are rejected by the primary solidifying phase and migrate into interdendritic regions. Additionally, the images reveal mechanical twins, which are associated with the internal stress field generated during cooling. These stresses arise from volumetric shrinkage of the Cu-Sn matrix during solidification and are counteracted by the incompressibility of molten Pb [18]. Due to its immiscibility with Cu and its lower melting point, Pb remains liquid during the final stages of cooling, migrating towards microvoids and channels and eventually forming a Pb-enriched outer layer. The resulting microstructure reflects key solidification dynamics, including thermal gradients, differential solidification rates, and phase separation governed by the limited solubility of Pb in Cu These observations highlight the function of Pb not merely as an alloying element, but as a separate phase whose physical behavior during casting and cooling significantly impacts the mechanical and structural characteristics of the finished artifact.

A schematic representation of the sequential stages underlying the formation of the above-mentioned phenomenon is presented below in Figure 11.

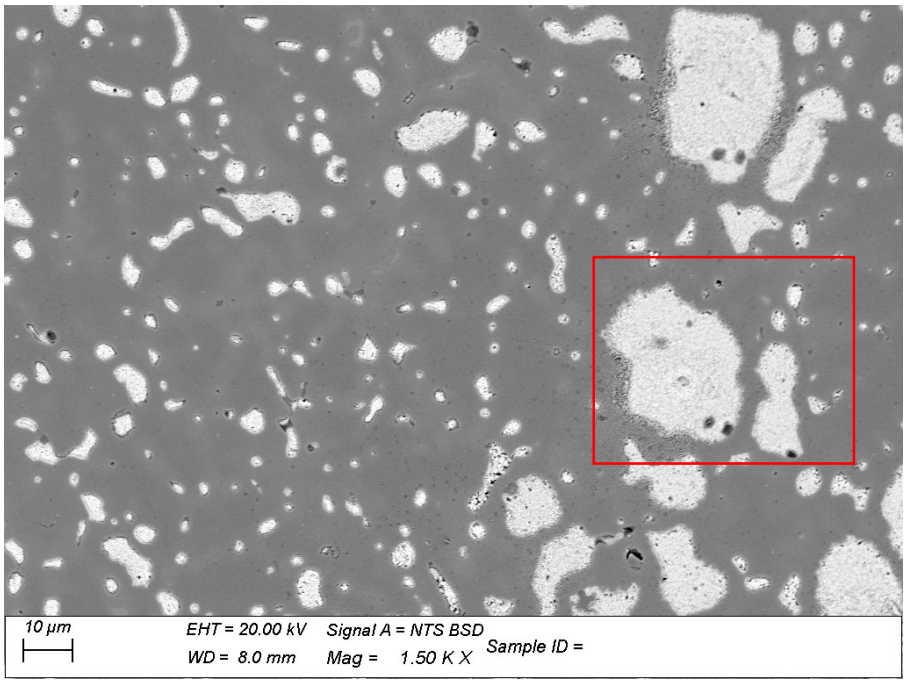



**Figure 6.** SEM image: Herc_1005. The red-marked box highlights the Pb nodules dispersed within the matrix, because the insolubility of the lead.

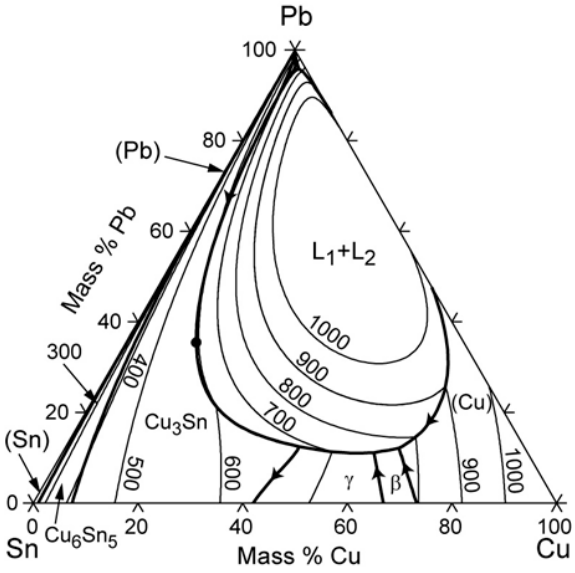



**Figure 7.** Ternary diagram phases Cu-Sn-Pb.

Lead, as stated before, has a key role in the manufacturing process of the statuary: it helps the alloy's castability by facilitating the manufacturing techniques processes. Its inclusion also helps reduce costs by decreasing the amount of Sn required, which is more expensive and difficult to find, and lastly mitigates issues within the *chaîne opératoire* because an excess of tin can embrittle the alloy, making it more difficult the workability of the same.

The patina that uniformly covers the surface, which at first macroscopic observation appeared thick with variable coloration depending on the statuette, was initially examined under the LOM. This patina is the natural result of the reaction between the elements in the alloy and various external agents present in the deposition environment [19]. A more in-depth analysis, such as Raman spectroscopy, would be necessary to determine its nature and chemical composition.

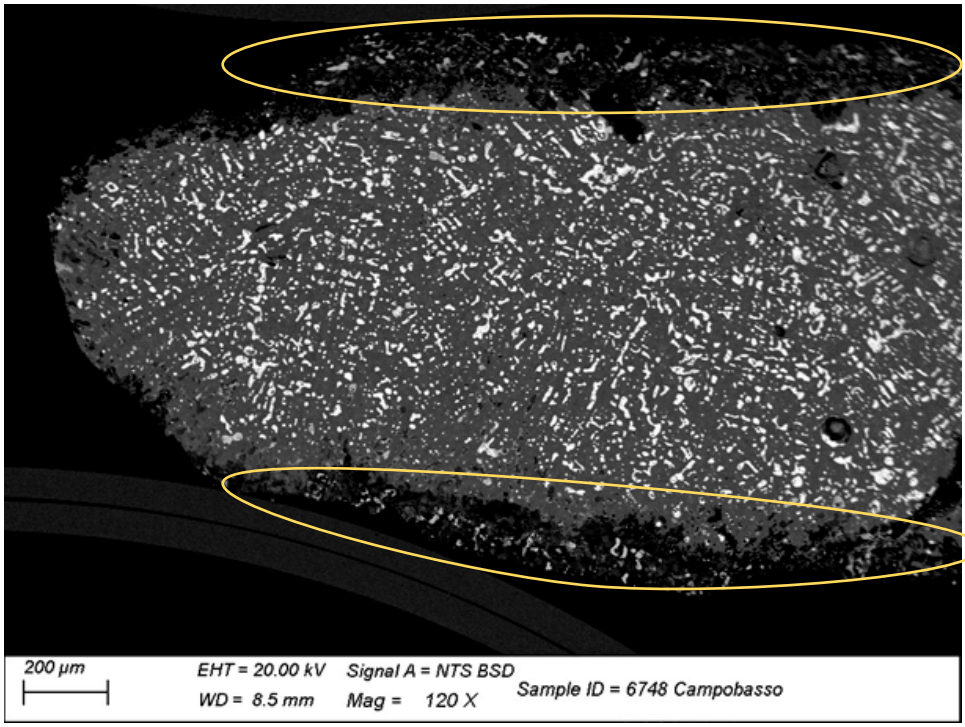



**Figure 8.** SEM image, Herc_6748. Highlighted in a golden-marked circle is the sponge structure due to the depletion of lead.

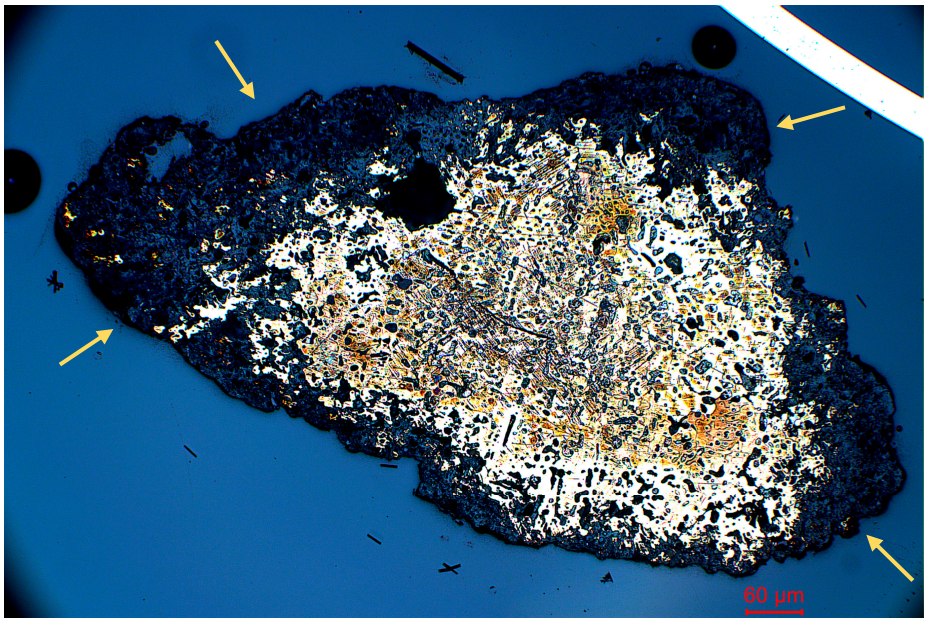



**Figure 9.** LOM image: Brightfield, Herc_6748, 100×, etched with alcoholic ferric chloride solution. Highlighted in golden arrows is the enrichment of lead at the external surface of the sample.

However, based on LOM observation alone, different corrosion products can be noted (Figure 12), with colors ranging from red to reddish-orange, green, and blue, often accompanied by a distinct stratification of these products. Generally, all the most observed corrosion products associated with Cu-based alloys emerge due to oxygen and interactions with agents in the deposition environment, such as specific pH conditions, organic components (e.g., sulfur-rich compounds), and soil moisture [20].

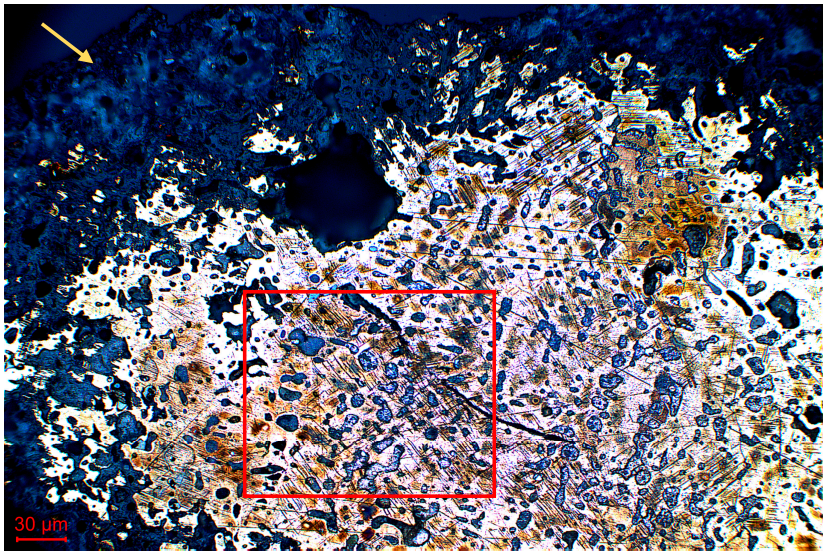



**Figure 10.** LOM image: Brightfield, Herc_6748, 200×, Etched with alcoholic ferric chloride solution. Highlighted in a golden-marked arrow in the enrichment of the lead at the external part of the sample. In the inner core of the sample are noticeable mechanical twins (within a red-marked box) due to the stress of the thermal contraction.

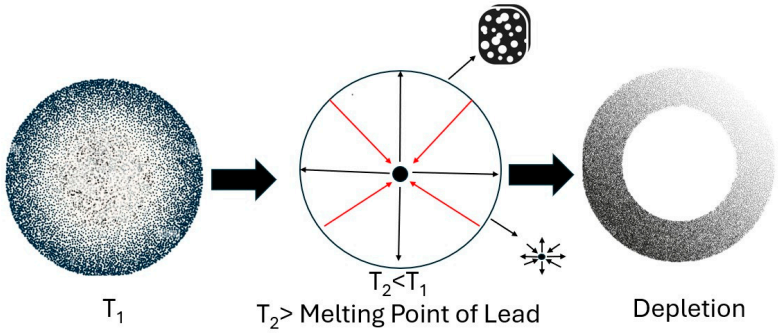



**Figure 11.** Illustrative scheme showing how thermal gradients above the melting point of lead promote the migration of molten Pb toward the surface, resulting in surface enrichment and internal depletion.

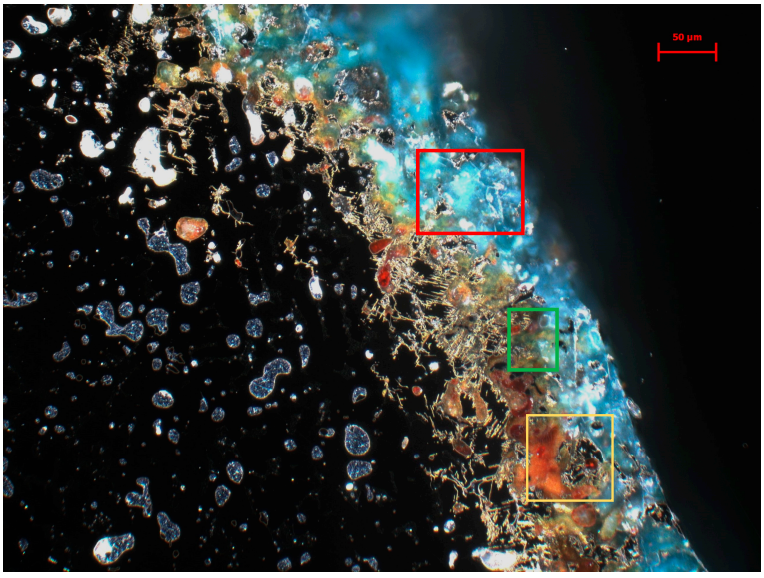



**Figure 12.** LOM image: Darkfield, Herc_58342, 200×. The corrosion products are highlighted within the red-marked, green-marked, and golden-marked boxes, because of their different nature and possibly different composition.

## 4. Discussion and Conclusions

*Compositional Analyses*

The composition of an alloy is a central factor in joint research efforts between archaeology and the fields of chemistry and materials science. This multidisciplinary approach is a valuable asset in cultural heritage studies. Initial typological analysis by an archaeologist can provide insights into an artifact's potential period, yet compositional analysis often offers further support. The acquisition of compositional data from metallic archaeological artifacts enables the delineation of a historical timeframe, founded in the existing literature; the alloy's constituent elements serve as chronological markers, reflecting the technological advancements in metals extraction, smelting, and artifact production during specific historical periods [21]. The alloy commonly found in both small and large statuary is a ternary alloy, primarily composed of copper (Cu) with concentrations ranging from 70 wt% to 80 wt%, with tin (Sn) and lead (Pb) as alloying elements; both Sn and Pb reduce the alloy's melting point. According to Amendola et al. [22], Pb and Sn have a synergic effect on castability due to the increase in capillarity and to the intrinsic impact of Pb on the thermal contraction during the cooling process, which is the origin of the enhanced ability to replicate details of the mold. Lead also reduces the melting temperature but has a poor effect on the mechanical properties, while it enhances the machinability. Above the limit of ca. 6 wt%, it has a detrimental effect on surface finishing. Adding Sn only dissolves in Cu lattice and thus has an impact on the mechanical properties. Sn also affects the color of the alloy, passing from reddish (pure copper) to goldish. The impact of Pb on color is more related to the Pb nodules visible on the surface. According to their size, it could result in adding a light grey to the Cu-Sn color to obtain a silvery color if large nodules are homogeneously spread. Tin to copper significantly increases the alloy's hardness [23], and the enhancement of castability is also related to the fluidity; according to the maintenance of the same casting temperature, if the melting is lower, the fluidity increases. Incorporating Pb also allowed for a reduction in the amount of tin required, a beneficial adjustment since tin was both more expensive and harder to obtain than lead.

This work represents the first systematic approach to the study of ancient metallic materials in the *Molise* region (Italy), intending to initiate metallurgical and compositional research on artifacts that had not previously been subjected to chemical, material or metallurgical analyses. The investigation focused on the compositional and metallographic analyses of a group of twenty-five votive statuettes of Hercules, dated between the 5th and 1st centuries BCE, and currently housed in the National Archaeological Museum of *Campobasso* (Italy). The goal was to better understand the technological practices, material choices, and craftsmanship of the metalworking workshops of the time. Initial compositional analyses were carried out using portable X-ray fluorescence spectroscopy (p-XRF), a non-invasive technique that provided a preliminary screening of the surface elemental composition of the statuettes. The data revealed considerable surface compositional variability, especially in the concentration of Sn and Pb. In several cases, significant surface enrichment in Sn was observed, which can be attributed to selective dealloying processes during corrosion, known as decuprification, where Cu dissolves preferentially compared to Sn, leaving behind a Sn-enriched surface layer [24]. In other samples, a surface enrichment in Pb was noted, a less commonly observed phenomenon likely resulting from segregation and migration of lead during solidification and subsequent post-depositional redistribution in the outer layers.

To complement the p-XRF analyses, micro-destructive sampling was performed on carefully selected statuettes based on their state of preservation and typological representativeness. Compositional analyses, carried out using Scanning Electron Microscopy (SEM), confirmed that the figurines were produced using a ternary Cu-Sn-Pb alloy, with tin

contents typically ranging between 5 wt% and 12 wt%, in some cases with lead contents exceeding 20 wt%. These tin levels are broadly consistent with bronze alloy formulations observed from the Middle Bronze Age onward, when the deliberate addition of tin, generally between 8 wt% and 12 wt%, became a standardized practice to optimize strength and casting behavior. Such ratios reflect a technological evolution from earlier, more variable bronze compositions towards alloys designed to balance hardness, ductility, and workability [25]. In the case of the statuettes under analysis, this choice, together with high Pb content, suggests sophisticated control over alloying practices, likely aimed at achieving specific mechanical and aesthetic properties suited for votive productions The high Pb content, suggests a deliberate addition of Pb to the alloy, likely to improve castability, lower the melting point, and enable finer detail reproduction during lost wax casting.

This also led to specific metallurgical phenomena, most notably marked segregation of Pb during the final stages of solidification. Since lead is insoluble in the copper matrix and has a significantly lower melting point (327 °C), it remains in the liquid phase while the Cu-Sn alloy solidifies. This results in a microstructure characterized by porosity and Pb-rich zones, which tend to accumulate along grain boundaries or in interdendritic cavities [26]. A sponge appearance of the metallic matrix was observed, with Pb inclusions that can lead to increased brittleness of the material. As the alloy cools, the volumetric shrinkage of the matrix creates contraction forces that act upon the still molten Pb. Being incompressible in its molten state, the lead expelled into the adjacent cavities or cracks, where it rapidly solidifies, forming the characteristic leaded skin. This phenomenon is macroscopically visible as grays, led colored hue, and microscopically as bands or surface zones with high Pb concentration. Moreover, the presence of mechanical twins observed in some metallographic sections suggests that thermal stress during cooling triggered localized plastic deformation in the matrix, especially near Pb inclusions [27].

Macroscopically, the patinas appear thick and evenly distributed across the entire surface of the statuettes. Light Optical Microscopy (LOM) of sampled sections revealed stratified corrosion products with varying coloration, indicative of prolonged and complex alteration processes. Plans include integrating these observations with more detailed compositional analyses using Raman spectroscopy to precisely identify the chemical nature of the corrosion products (e.g., cuprite, chloride phases, basic carbonates).

This research will support the development of a tailored conservation protocol aimed at stabilizing and, where appropriate, restoring the artifacts. Additionally, corrosion studies using Raman spectroscopy and the reproduction of the statuettes through casting will be conducted to develop a conservation protocol, to create inclusive displays for museum audiences. In conclusion, this study showcases the potential of integrated material science, metallurgy, and chemistry in heritage studies.

**Author Contributions:** Conceptualization, C.C. and P.P.; methodology, C.C., P.P. and R.S., software, C.C. and P.P., validation, P.P. and D.D., formal analysis, C.C. and P.P., investigation, C.C., P.P. and D.D., resources, P.P. and D.D., data curation, C.C., P.P. and R.S., writing-original draft preparation, C.C., writing-review and editing, P.P., C.C., D.D. and R.S., visualization, C.C. and P.P., project administration P.P., D.D. and C.C., funding acquisition D.D. and P.P. All authors have read and agreed to the published version of the manuscript.

**Funding:** This work was made possible within the Project "Archeometallurgy of Pentrian Samnium" project, financed by the Italian Ministry of Culture within the "Three-year program 2021–2023 pursuant to art. 1 paragraphs 9 and 10 of Law 23 December 2014, n. 190 YEARS 2021–2023"—Ministerial Decree 16 December 2021, rep. 450, managed by Archaeological Park of Sepino-Regional Directorate of National Museums of Molise.

**Data Availability Statement:** The original contributions presented in this study are included in the article. Further inquiries can be directed to the corresponding author.

**Acknowledgments:** I wish to express my sincere gratitude to Paolo Piccardo, Davide Delfino, and Roberto Spotorno for their invaluable guidance and insightful advice throughout this research. I am also indebted to the Museo Archeologico Nazionale di Campobasso and the Direzione Regionale Musei Nazionali Molise for granting access to the collections and facilities. I would further like to acknowledge all collaborators for their contributions and support.

**Conflicts of Interest:** The authors declare no conflict of interest.

## References

1. Delfino, D. Il Museo Sannitico di Campobasso. In *Un Viaggio di 4.000 Anni Nella Storia del Sannio*; Segretariato Regionale del Ministero della cultura per il Molise: Campobasso, Italy, 2020.
2. Sogliano, A. *Il Museo Provinciale Sannitico di Campobasso:Inventario Degli Oggetti Antichi*; Tip. della Regia Università: Naples, Italy, 1889; p. 208.
3. IL MUSEO SANNITICO DI CAMPOBASSO Catalogo Della Collezione Provinciale—CARSA Edizioni. Available online: https://www.carsaedizioni.it/prodotto/il-museo-sannitico-di-campobasso-catalogo-della-collezione-provinciale/ (accessed on 28 November 2025).
4. Delfino, D.; Carbonara, V. *The Cult of Hercules Between 6th and 2th Century in the Bronze Statuary of the Samnite Museum of Campobasso (Molise, Italy)*; Dacica: Alun, Romania, 2020.
5. Sîrbu, V.; Peţan, A. Temples and cult places from the second Iron Age in Europe. In *Proceedings of the 2nd International Colloquium "Iron Age Sanctuaries and Cult Places at the Thracians and Their Neighbours", Alun, Romania, 7–9 May 2019*; Dacica: Alun, Romania, 2020.
6. Piccardo, P.; Mille, B.; Robbiola, L. 14—Tin and copper oxides in corroded archaeological bronzes. In *Corrosion of Metallic Heritage Artefacts*; Dillmann, P., Béranger, G., Piccardo, P., Matthiesen, H., Eds.; European Federation of Corrosion (EFC) Series; Woodhead Publishing: Cambridge, UK, 2007; Volume 48, pp. 239–262. Available online: https://www.sciencedirect.com/science/article/pii/B978184569239150014X (accessed on 16 July 2025).
7. Ghosh, A. Segregation in cast products. *Sadhana* **2001**, *26*, 5–24. [CrossRef]
8. Harries, D.R.; Marwick, A.D. Non-Equilibrium Segregation in Metals and Alloys. *Philos. Trans. R. Soc. Lond. Ser. Math. Phys. Sci.* **1980**, *295*, 197–207.
9. Khoza, I. *NMC 313—Materials Science Practical 1: Segregation During Solidification*; Academia: San Francisco, CA, USA, 2016.
10. Oudbashi, O.; Hasanpour, A.; Davami, P. Investigation on corrosion stratigraphy and morphology in some Iron Age bronze alloys vessels by OM, XRD and SEM–EDS methods. *Appl. Phys. A* **2016**, *122*, 262. [CrossRef]
11. Silveira, P.; Falcade, T. Applications of energy dispersive X-ray fluorescence technique in metallic cultural heritage studies. *J. Cult. Herit.* **2022**, *57*, 243–255. [CrossRef]
12. Oudbashi, O.; Emami, S.M.; Ahmadi, H.; Davami, P. Micro-stratigraphical investigation on corrosion layers in ancient Bronze artefacts by scanning electron microscopy energy dispersive spectrometry and optical microscopy. *Herit. Sci.* **2013**, *1*, 21. [CrossRef]
13. Abdelbar, M.; El-Shamy, A.M. Understanding soil factors in corrosion and conservation of buried bronze statuettes: Insights for preservation strategies. *Sci. Rep.* **2024**, *14*, 19230. [CrossRef] [PubMed]
14. Zhang, Z.; Deng, C. Grain boundary interstitial segregation in substitutional binary alloys. *Acta Mater.* **2025**, *291*, 121019. [CrossRef]
15. Assunção, M.; Vynnycky, M. On macrosegregation in a binary alloy undergoing solidification shrinkage. *Eur. J. Appl. Math.* **2024**, *35*, 40–61. [CrossRef]
16. Cui, H.B.; Guo, J.J.; Su, Y.; Ding, H.S.; Wu, S.P.; Bi, W.S.; Xu, D.M.; Fu, H.Z. Microstructure evolution of Cu-Pb monotectic alloys during directional solidification. *Trans. Nonferrous Met. Soc. China* **2006**, *16*, 783–790. [CrossRef]
17. Liu, X.; Zheng, J.; Li, X.; Niu, C.; Peng, L.; Wan, F.; Liu, Z.; Zuo, Y.; Xue, C.; Cheng, B. Investigation of lead surface segregation during germanium–lead epitaxial growth. *J. Mater. Sci.* **2020**, *55*, 4762–4768. [CrossRef]
18. Inverse Segregation—An Overview | ScienceDirect Topics. Available online: https://www.sciencedirect.com/topics/engineering/inverse-segregation (accessed on 16 July 2025).
19. Robbiola, L.; Portier, R. A global approach to the authentication of ancient bronzes based on the characterization of the alloy–patina–environment system. *J. Cult. Herit.* **2006**, *7*, 1–12. [CrossRef]
20. Nord, A.G.; Mattsson, E.; Tronner, K. Factors Influencing the Long-term Corrosion of Bronze Artefacts in Soil. *Prot. Met.* **2005**, *41*, 309–316. [CrossRef]

21. Piccardo, P.; Ghiara, G.; Vernet, J.M. Mise en Œuvre des Alliages Cuivreux: Faire Parler le Métal Grâce à la Science des Matériaux. 2017. Available online: https://science.ulysseus.eu/records/qn5g7-jtn19 (accessed on 27 October 2025).
22. Piccardo, P.; Amendola, R.; Adobati, A.; Faletti, C. Studio Della Fluidità Di Leghe A Base Rame. *Metall. Ital.* **2009**, *101*, 31.
23. Kohler, F.; Germond, L.; Wagnière, J.D.; Rappaz, M. Peritectic solidification of Cu–Sn alloys: Microstructural competition at low speed. *Acta Mater.* **2009**, *57*, 56–68. [CrossRef]
24. Eggert, G. 'Copper and Bronze in Art' and the Search for Rare Corrosion Products. *Heritage* **2023**, *6*, 1768–1784. [CrossRef]
25. Nessel, B.; Brügmann, G.; Frank, C.; Marahrens, J.; Pernicka, E. Tin Provenance and Raw Material Supply—Considerations about the Spread of Bronze Metallurgy in Europe. *Metalla* **2019**, *24*, 65–72. [CrossRef]
26. Kumar, S.; Handwerker, C.A.; Dayananda, M.A. Intrinsic and Interdiffusion in Cu-Sn System. *J. Phase Equilibria Diffus.* **2011**, *32*, 309–319. [CrossRef]
27. Macrosegregation—An Overview | ScienceDirect Topics. Available online: https://www.sciencedirect.com/topics/engineering/macrosegregation (accessed on 16 July 2025).

**Disclaimer/Publisher's Note:** The statements, opinions and data contained in all publications are solely those of the individual author(s) and contributor(s) and not of MDPI and/or the editor(s). MDPI and/or the editor(s) disclaim responsibility for any injury to people or property resulting from any ideas, methods, instructions or products referred to in the content.